

# Conservative Constraints on Dark Matter from the Fermi-LAT Isotropic Diffuse Gamma-Ray Background Spectrum

Kevorg N. Abazajian, Prateek Agrawal, and Zackaria Chacko  
*Maryland Center for Fundamental Physics, Department of Physics,  
 University of Maryland, College Park, Maryland 20742 USA*

Can Kilic

*Department of Physics & Astronomy, Rutgers University, Piscataway, NJ 08854, USA*

We examine the constraints on final state radiation from Weakly Interacting Massive Particle (WIMP) dark matter candidates annihilating into various standard model final states, as imposed by the measurement of the isotropic diffuse gamma-ray background by the Large Area Telescope aboard the Fermi Gamma-Ray Space Telescope. The expected isotropic diffuse signal from dark matter annihilation has contributions from the local Milky Way (MW) as well as from extragalactic dark matter. The signal from the MW is very insensitive to the adopted dark matter profile of the halos, and dominates the signal from extragalactic halos, which is sensitive to the low mass cut-off of the halo mass function. We adopt a conservative model for both the low halo mass survival cut-off and the substructure boost factor of the Galactic and extragalactic components, and only consider the primary final state radiation. This provides robust constraints which reach the thermal production cross-section for low mass WIMPs annihilating into hadronic modes. We also reanalyze limits from HESS observations of the Galactic Ridge region using a conservative model for the dark matter halo profile. When combined with the HESS constraint, the isotropic diffuse spectrum rules out all interpretations of the PAMELA positron excess based on dark matter annihilation into two lepton final states. Annihilation into four leptons through new intermediate states, although constrained by the data, is not excluded.

## I. INTRODUCTION

The identity of the dark matter has remained a fundamental unsolved problem in cosmology and particle physics for nearly eighty years [1]. The likelihood of new physics near the electroweak scale suggests a particle dark matter candidate of mass  $\sim 100$  GeV. A weak-scale interaction strength for such a particle can naturally produce a relic abundance at the observed dark matter density. Such a weakly-interacting massive particle (WIMP) arises in supersymmetric extensions of the standard model as well as other beyond the standard model extensions. For a review of particle dark matter candidates, see, e.g., Refs. [2, 3].

Thermal production of dark matter prefers a scale of the dark matter annihilation cross-section at  $\langle\sigma_A v\rangle \approx 3 \times 10^{-26} \text{ cm}^3 \text{ s}^{-1}$ . This scale predicts a potentially detectable gamma-ray photon signal from annihilations in local and cosmological dark matter structures, e.g., see Ref. [4]. Annihilation channels directly to photon pairs produce a distinctive  $\gamma$ -ray spectral line, while channels to charged standard model particles produce an associated continuum emission of  $\gamma$ -rays from bremsstrahlung radiation and in hadronization via  $\pi^0 \rightarrow \gamma\gamma$ . The Large Area Telescope (LAT) aboard the recently launched Fermi Gamma-Ray Space Telescope has significant sensitivity to such  $\gamma$ -ray radiation from dark matter annihilation. The sensitivity of Fermi-LAT to an annihilation signal from the Galactic center (GC), Galactic satellites

and the isotropic diffuse signal was reviewed in Baltz et al. [5].

Recent Fermi-LAT observations have led to constraints on dark matter annihilation, including observations of dwarf galaxies analyzed by the Fermi-LAT Collaboration [6, 7], as well as analyses of public data of the total sky flux [8], and public data from selected portions of the sky [9]. Most recently, the Fermi-LAT collaboration released the spectrum from the isotropic diffuse background in  $\gamma$ -rays [10]. Here, we use the Fermi-LAT Collaboration derived diffuse-photon spectrum in this work to place constraints on dark matter annihilation channels. Depending on the background estimation, the relative sensitivity of these methods varies.

In this work, we constrain the partial cross section for dark matter annihilation to various particle anti-particle standard model final states using the diffuse isotropic  $\gamma$ -ray photon spectrum from the Fermi-LAT [10]. The Fermi-LAT isotropic diffuse spectrum uses enhanced event simulation modeling that improves the background rejection in the observations by a factor of 1.3-10. Therefore, we expect the spectrum to be a stringent constraint on dark matter annihilation. The errors on the estimate of the diffuse isotropic background come from systematic errors in modeling foreground Galactic diffuse  $\gamma$ -ray emission. The isotropic diffuse background could include a dark matter annihilation signal, yet also has contributions from unresolved active galactic nuclei, starburst galaxies and  $\gamma$ -ray bursts, as well as any truly diffuse

components in large scale structure. In total, the modeling of the Galactic diffuse emission, as well as the extragalactic  $\gamma$ -ray emission processes, are the ultimate observational limits to the sensitivity of the isotropic diffuse background to a dark matter signal.

Since Cold Dark Matter (CDM) particle candidates such as the WIMPs considered here produce cusped halos [4, 11], in applying our constraints, we use conservative models for the expected dark matter profile density distribution which are consistent with the cusped profiles produced by such CDM candidates. We also apply this requirement to update limits from existing constraints from observations of the GC ridge by HESS.

The Fermi-LAT collaboration performed a similar analysis of the constraints from the diffuse background observations [12]. That work did not include the minimal Galactic contribution that is necessarily present in the observation, and is therefore less stringent than the limits presented here. Previous work along these lines prior to Fermi-LAT data include limits from older  $\gamma$ -ray observations with a subset of standard model channels: Bell & Jacques [13] examined constraints on the branching ratio to  $e^+/e^-$  with the EGRET, CGRO, HESS and CELESTE data, and Mack et al. [14] applied constraints on lines in the case of the two-photon channel with a similar set of data. With the dawn of the Fermi-LAT data, constraints from all-sky and diffuse flux limits have been made with public data. Cirelli et al. [9] use the total flux from specific sky regions to constrain dark matter annihilations using conservative models for the dark matter halo profile. They include  $\gamma$ -rays arising from inverse-Compton scattering (ICS) of annihilation products on cosmic microwave background and inter-stellar photons. In a similar analysis, Pappucci & Strumia [8] find limits to dark matter annihilation modes from a full-sky analysis of the public Fermi-LAT data, including final state radiation limits as well as ICS, with no reduction of the sky flux due to foreground galaxy and point source removal. Therefore, their constraints are not as stringent as ours or those in Ref. [9]. Ref. [8] also overstates MW halo profile dependencies by adopting isothermal halo profile models, which, as we discuss below, are inconsistent with the CDM structure formation paradigm for a WIMP candidate.

There has been considerable interest in the possibility of dark matter annihilation as being the source of the excess cosmic ray positron fraction at  $\sim 10$ -100 GeV observed by HEAT<sup>1</sup> [15], AMS-01<sup>2</sup> [16] and PAMELA<sup>3</sup> [17], where  $e^+/e^-$  pairs are produced directly or indirectly in a dark matter particle pair annihilation cascade [18, 19]. In addition, features in the higher-energy  $10^2$ -

$10^3$  GeV positron spectrum seen by ATIC<sup>4</sup> [20] and Fermi-LAT [21] are also consistent with the dark matter annihilation interpretations of in the lower energy positron excess data [22–24]. In order to achieve the dark matter annihilation rate required for these  $e^+/e^-$  signals that may be consistent with the expected thermal production cross section, and to avoid an excess in anti-proton observations, the annihilation rate can be enhanced through a low-energy Sommerfeld enhancement, and limited to leptonic modes with a  $< 1$  GeV dark-force carrying particle [25–28]. Such an enhanced cross-section from a new force is in tension with detailed calculations of the relic abundance of the dark matter, so that such a candidate may not contribute to all of the dark matter [29–31], and are also constrained by nonthermal distortions of the CMB [29] and asphericity observed in dark matter halos [30].

These models are also constrained by corresponding Fermi-LAT  $\gamma$ -ray observations of dwarf galaxies [7], the total sky flux [8], portions of the sky [9], Galactic radio synchrotron emission [32], the neutrino flux from the GC as observed by SuperKAMIOKANDE [24], and atmospheric Cerenkov observations of  $\gamma$ -rays from dwarf galaxies [33]. Hütsi et al. [34] have used diffuse  $\gamma$ -ray observations by EGRET to constrain dark matter models that can explain the PAMELA data, but as we explain below, with more optimistic assumptions for the low mass halo cutoff and extragalactic signal. The PAMELA, HEAT, and Fermi  $e^+/e^-$  signals are also consistent with high-energy  $e^+/e^-$  emission from pulsars and supernova remnants [35–38]. Here, we show how the dark matter annihilation interpretation of these signals is in conflict with the observed isotropic diffuse flux spectrum of Fermi-LAT in combination with other constraints for two-body standard model particle final states, and constrains scalar or vector boson mediated four-lepton final states.

## II. ANNIHILATION SIGNAL

A robust calculation of the expected final state radiation from dark matter annihilation requires accurate quantification of the dark matter source as well as the products in the final state  $\gamma$ -ray radiation chain. The observable flux of photons per solid angle for a specific annihilation channel with cross section  $\langle \sigma_{Av} \rangle$  is

$$\frac{d\Phi_\gamma}{dE} = \frac{\langle \sigma_{Av} \rangle}{2} \frac{\mathcal{J}_{\Delta\Omega}}{J_0} \frac{1}{\Delta\Omega_{\text{obs}} m_\chi^2} \frac{dN_\gamma}{dE}, \quad (1)$$

where  $\mathcal{J}_{\Delta\Omega}/J_0$  is the normalized integral of mass density squared of the dark matter in the field of view,  $dN_\gamma/dE$  is

<sup>1</sup> High Energy Antimatter Telescope balloon experiment

<sup>2</sup> The Alpha Magnetic Spectrometer experiment

<sup>3</sup> Payload for Antimatter Matter Exploration and Light-nuclei Astrophysics, <http://pamela.roma2.infn.it>

<sup>4</sup> Advanced Thin Ionization Calorimeter, <http://atic.phys.lsu.edu/aticweb/>

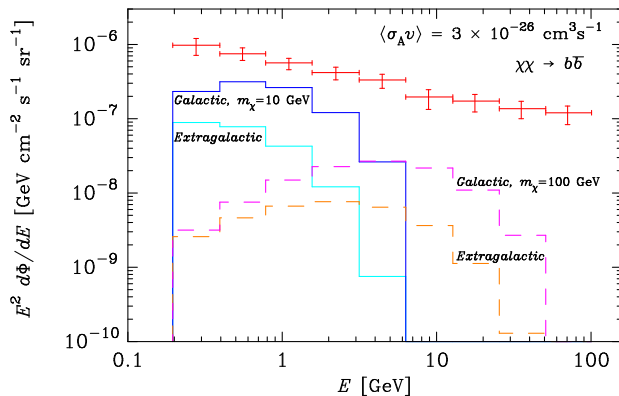


FIG. 1: Shown is the observed isotropic diffuse background spectrum observed by Fermi-LAT (points with errors), and representative models of the annihilation spectrum of the Galactic (upper) and extragalactic (lower) contributions from the channel  $\chi\chi \rightarrow b\bar{b}$  for  $m_\chi = 10$  GeV (solid), and for  $m_\chi = 100$  GeV (dashed). Both cases have the annihilation cross section  $\langle\sigma_A v\rangle = 3 \times 10^{-26} \text{ cm}^3 \text{ s}^{-1}$ .

the  $\gamma$ -ray spectrum per annihilation,  $m_\chi$  is the dark matter particle mass, and  $\Delta\Omega_{\text{obs}}$  is the observational solid angle in steradians. This relationship is dependent on the astrophysically-inferred dark matter density contribution in the field of view of an observation  $\mathcal{J}_{\Delta\Omega}$ , and the particle physics of the expected photon flux for a specific particle candidate annihilation mode,  $dN_\gamma/dE$ . Note that  $d\Phi_\gamma/dE$  is the total photon number flux per unit energy per unit steradian for a full sky observation, and when compared to the total photon count of the Fermi-LAT observation with  $|b| > 10^\circ$ , must be scaled to the field of view of that observation,  $\Delta\Omega_{\text{obs}} = 10.4 \text{ sr}$ .<sup>5</sup> The Fermi-LAT diffuse isotropic background spectrum observation as well as examples of the isotropic diffuse signal for both the Galactic and extragalactic contributions are shown in Fig. 1. We describe our methods in detail below.

### A. Particle Annihilation Event Modeling

For dark matter annihilations to two-body standard model final states, in order to obtain the average number of photons above a given energy per annihilation event and the differential number of photons at a given energy per annihilation event  $dN_\gamma/dE$ , we use Pythia 6.4 [39] to simulate both photon radiation off of charged particles as well as decays of particles such as the  $\pi^0$ . Specifically, we run Pythia to simulate an  $e^+e^-$  collision at a center of mass energy of  $2m_\chi$  through a  $Z'$  to a final state that corresponds to the annihilation products of the dark matter.

For certain final states such as  $gg$  we use an s-channel  $h$  rather than a  $Z'$ , as the corresponding decay process is already implemented in Pythia and does not need to be added by hand. For the  $hh$  final state we add a new decay channel for the  $Z'$ . We switch off initial state radiation such that all photons are emitted either radiatively off the final state particles or the decays of unstable particles such as mesons. We use the default Pythia cutoff values for photon emission: quarks are assumed not to radiate below a GeV, and leptons below 100 keV. We turn on the decays of particles which are not decayed with the default Pythia settings, such as muons, charged pions and kaons. Using a large sample of events for each final state and each value of  $m_\chi$ , the number of photons in the final state above a given energy are counted and averaged over the number of events, yielding the average number of photons above a given energy per annihilation event.

For dark matter annihilations to final states such as  $4e$  and  $4\mu$  through intermediate light scalars, we utilize the formulas given in Appendix A of Ref. [40]. For the four- $e$  final state, all photons originate from final state radiation off of the electrons. For the four- $\mu$  final state, photons can originate from final state radiation off of the muons, as well as from final state radiation off of electrons produced by the decay of the muons. Since dark scalars are by assumption light, the energy range over which photons can be radiated is narrow in the rest frame of the scalar. While in the center of mass frame of the dark matter annihilation some of these photons can still carry a significant fraction of the available energy, the average number of hard photons per annihilation event is significantly reduced in comparison to direct annihilation to a two-body standard model final state.

### B. Cold Dark Matter Halo Models

Thermally-produced dark matter particle candidates detectable in  $\gamma$ -rays are CDM particles whose primordial velocities are only determined by the initial gravitational perturbations. We therefore only consider dark matter halo models that arise in CDM cosmologies. In particular, density profiles of approximately the canonical Navarro-White-Frenk (NFW) profile are expected for the Milky Way (MW) dark matter halo [11], with profiles of the form

$$\rho_{\text{NFW}}(r) = \rho_s \left(\frac{r}{r_s}\right)^{-1} \left(1 + \frac{r}{r_s}\right)^{-2}, \quad (2)$$

where  $\rho_s$  is the characteristic density and  $r_s$  is the scale radius. Halos in simulations exhibit scatter about this profile [41]. We employ the NFW profile in order to allow for comparison to other work. However, higher resolution simulations of CDM halo formation have revealed a softening of the profile power law with decreasing radius that deviates slightly but significantly from NFW, with a logarithmic slope that decreases with radius [42, 43]. Called

<sup>5</sup> An earlier version of this paper incorrectly omitted this geometrical factor. We thank Julie McEnery, Michael Gustafsson, and the Fermi Collaboration for helping resolve this issue.

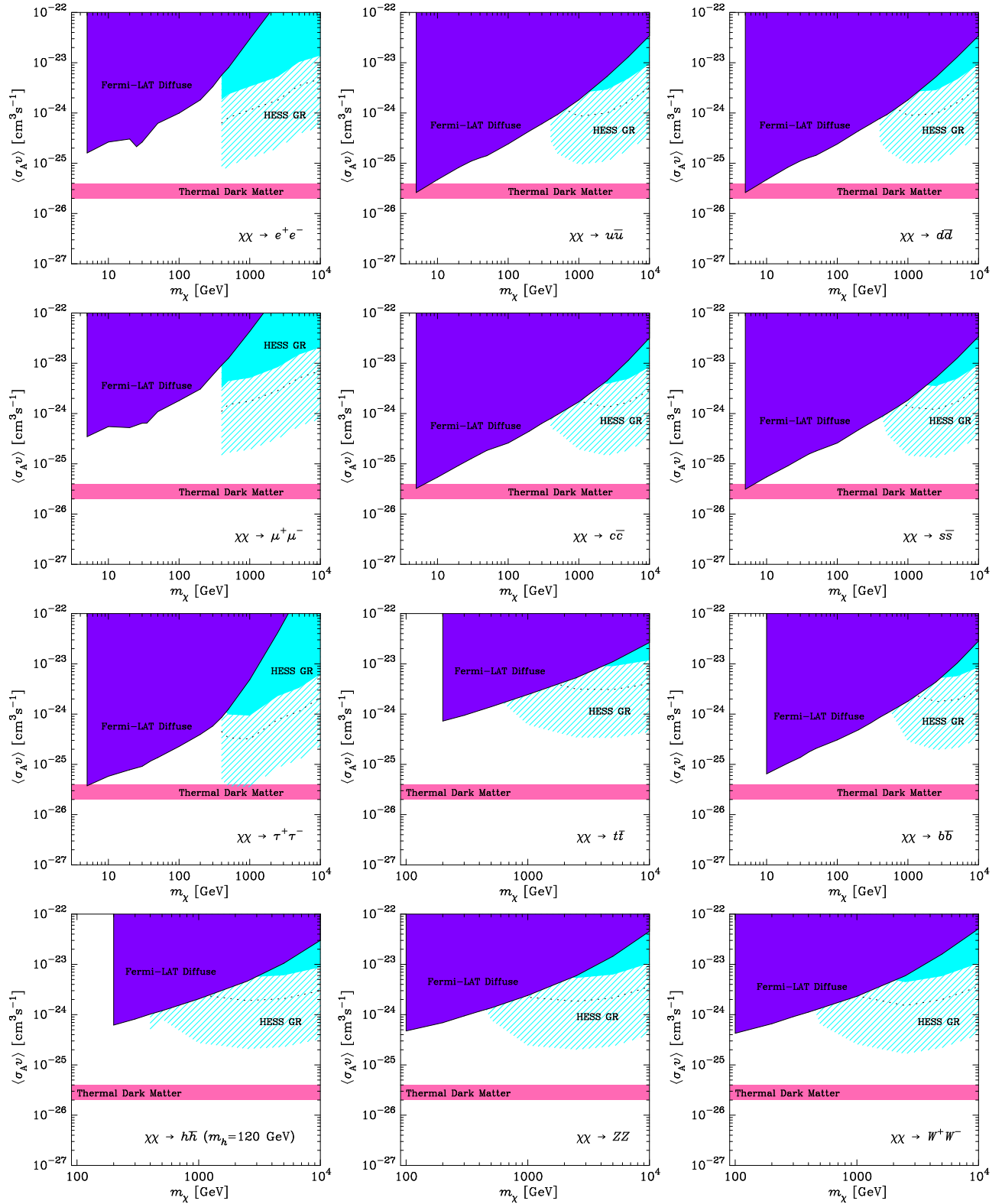


FIG. 2: Constraints on the partial cross section of annihilation of dark matter to quarks, leptons, gauge bosons and Higgs, for  $m_h = 120$  GeV. The regions are labeled by their corresponding constraining observations as described in the text: “Fermi-LAT Diffuse” from the Fermi-LAT isotropic diffuse  $\gamma$ -ray background. The regions labeled “HESS GR” are for three different cases, solid cyan using the conservative Einasto profile as described in the text, hashed cyan from the most stringent case, a low mass high concentration NFW profile, and the canonical  $\rho_\odot = 0.3 \text{ GeV cm}^{-3}$ ,  $R_\odot = 8.5 \text{ kpc}$  NFW profile as a dotted line for reference. All constraints are at 95% CL.

an Einasto profile, it is of the form

$$\rho_{\text{Einasto}}(r) = \rho_s \exp \left[ -\frac{2}{\alpha_E} \left( \left( \frac{r}{r_s} \right)^{\alpha_E} - 1 \right) \right], \quad (3)$$

where  $\alpha_E$  is fit by simulations to be roughly  $\alpha_E \approx 0.17 \pm 0.02$ . This profile shows this self-similar behavior to the resolution limit of the simulations at 100 kpc/h.

We choose conservative models the of dark matter halo profile in calculating  $\mathcal{J}_{\Delta\Omega}$  that are consistent with CDM in addition to observational constraints of the MW halo. The MW CDM halo profile has been constrained with dynamical measurements by Klypin et al. [44] and Battaglia et al. [45] using NFW-type halo profiles. Recent results by Catena & Ullio (CU) [46] have applied such dynamical constraints to NFW as well as Einasto profiles of the MW with a Markov-Chain Monte Carlo parameter exploration of the degeneracies in fit parameters in these models, providing the local (solar) density estimates of the MW halo as well as the global profiles for these halos. The results of CU allow using not only minimal models in MW halo mass, but variations in other parameters as well.

There exists an overwhelming amount of results from verified numerical simulations that halos in CDM cosmologies generally form cusped profiles of the form exemplified by the NFW and Einasto profiles [11, 47–49]. The original *ansatz* of CDM has been shown to be consistent with a large range of scales of observations, including the cosmic microwave background [50], large scale clustering of galaxies and dark matter,  $\sim 100$  Mpc/h, in the Sloan Digital Sky Survey [51], to the small scales of the intergalactic medium measured in the Lyman- $\alpha$  forest,  $\sim 50$  kpc/h [52–54]. We do not consider isothermal and Burkert profiles, since cored profiles of these forms never arise in CDM halo formation simulations of halos of the mass of the MW. We also do not consider the more shallow-cusped “Kravtsov” profiles originally from Ref. [55] since following work by the same authors found sufficient force resolution but insufficient mass resolution in the original simulations, leading to the spurious shallower profiles [56].

### C. Galactic Center Observations

For comparison, we include constraints from observations towards the center of our Galaxy. The integrated mass density squared along line-of-sight  $x$  towards Galactic coordinates  $(b, \ell)$  from the GC is

$$\mathcal{J}(b, \ell) = J_0 \int_{x_{\min}}^{x_{\max}} \rho^2(r_{\text{gal}}(b, \ell, x)) dx, \quad (4)$$

where  $J_0 \equiv 1/\left[8.5 \text{ kpc} (0.3 \text{ GeV cm}^{-3})^2\right]$  is a normalization that makes  $\mathcal{J}$  unitless and cancels in final expressions for observables, and

$$r_{\text{gal}}(b, \ell, x) = \sqrt{R_{\odot}^2 - 2xR_{\odot} \cos(\ell) \cos(b) + x^2}. \quad (5)$$

The lower and upper limit of the integration  $x_{\min}$ ,  $x_{\max}$  are set by whether it’s the MW or an extragalactic halo. The limits chosen are somewhat arbitrary since galactic halos are embedded and continuous with a network of lower-density filamentary structures. However, the contribution beyond the scale radius is minimal, and we simply choose a cutoff at the nominal virial radius for the MW. The average of the integrated mass density is

$$\mathcal{J}_{\Delta\Omega} = \frac{1}{\Delta\Omega} \int_{\Delta\Omega} \mathcal{J}(b, \ell) d\Omega, \quad (6)$$

over the relevant sky region, where  $\Delta\Omega$  is the angular size of the observation region. Although the NFW profile is divergent at the GC, the average over a finite observation region is insensitive to the exact nature of the inner cusp for the  $\gamma$ -ray observations here. We regularize the NFW profile by fixing a constant density of the profile within  $r_{\text{halo}} < 10^{-10}$  kpc to the density at  $\rho(r_{\text{halo}} = 10^{-10} \text{ kpc})$  in Eq. 6, which has negligible effect on the integrated average.

One of the most stringent limits on dark matter annihilation arise from observations of the MW Galactic center ridge (GR) by the High Energy Stereoscopic System (HESS) telescope [57], an array of atmospheric Čerenkov telescopes in operation in Namibia<sup>6</sup> [13, 14, 24, 32, 58–60]. The HESS GR observations are for an angular region  $-0.8^\circ < \ell < 0.8^\circ$  and  $-0.3^\circ < b < 0.3^\circ$ . We integrate Eq. (6) directly, through a Monte-Carlo integration method over the nontrivial geometry. Note that in HESS GR observation subtracted a background from a region  $-0.8^\circ < \ell < 0.8^\circ$  and  $0.8^\circ < b < 1.5^\circ$  to remove cosmic ray backgrounds. This also removes any concurrent dark matter signal in the background region, which we incorporate appropriately by integrating the signal from the background subtracted region  $-0.8^\circ < \ell < 0.8^\circ$  and  $0.8^\circ < b < 1.5^\circ$  numerically, also through a Monte Carlo integration method for the arbitrary geometry.<sup>7</sup> The full Monte Carlo integration particularly affects the Einasto profile case due to the shallower Einasto profile which falls off more slowly than NFW in the background region, and therefore increases the background subtraction.

We calculate extremal cases for  $\mathcal{J}_{\Delta\Omega, \text{HGR}}$  towards the

<sup>6</sup> <http://www.mpi-hd.mpg.de/hfm/HESS/HESS.html>

<sup>7</sup> Note that we do not adopt an often-employed circular area approximation for the HESS GR observational geometry, or a point approximation for the background subtraction, e.g. in [13, 14]. The circular approximation underestimates the signal by approximately a factor of two, primarily because the observational area is overestimated while the signal is centrally concentrated. The circular area approximation with angle  $\psi = 0.8^\circ$  has  $\Delta\Omega_{\text{circ}} = 2\pi(1 - \cos\psi) = 6.1 \times 10^{-4}$  sr while the HESS GR observation was over an area  $\Delta\Omega_{\text{HESS}} = 2.9 \times 10^{-4}$  sr. The background approximation of a point subtraction at  $\psi = 0.8^\circ$  overestimates the background integral, yet this is partially offset by the smaller area of the background  $\Delta\Omega_{\text{HESS, bg}} = 3.4 \times 10^{-4}$  sr than in the point approximation.

HESS GR field of view, such that

$$\mathcal{J}_{\Delta\Omega, \text{HGR}} = \begin{cases} 555 & \text{CU Einasto Minimum} \\ 1050 & \text{Battaglia NFW Low Mass} \\ 2500 & \text{CU NFW Low } c \\ 13100 & \text{Battaglia NFW High Mass} \\ 14700 & \text{CU NFW High } c. \end{cases} \quad (7)$$

For the minimal Einasto case, we use a softer conservative value of the log-slope that is consistent with the fits of CU, with  $\alpha_E = 0.22$ ,  $r_s = 21$  kpc,  $r_\odot = 8.28$  kpc and  $\rho_\odot = 0.385 \text{ GeV cm}^{-3}$  which are the values we adopt as our conservative minimal case of the MW halo profile in the HESS GR field of view. Our adopted maximally stringent case is the NFW profile from CU which has the highest concentration,  $c$ . High concentration enhances the signal toward the GC, yet is anti-correlated with halo mass [46], therefore corresponding to a low mass MW halo, with  $c = 24.6$  and  $M_{\text{vir}} = 1.23 \times 10^{12} M_\odot$ . The CU NFW low  $c$  case has  $c = 13.9$  and  $M_{\text{vir}} = 1.86 \times 10^{12} M_\odot$  (we do not employ this model in our constraints). Both CU NFW profiles adopt  $r_\odot = 8.28$  kpc. The high and low mass NFW cases from Battaglia et al. [45] correspond to the 68% CL limits of the MW halo model:  $M_{\text{vir}} = 0.6 \times 10^{12} M_\odot$  (low mass),  $M_{\text{vir}} = 2.0 \times 10^{12} M_\odot$  (high mass). Both of these cases have other parameters fixed at  $R_{\text{vir}} = 255 \text{ kpc}$ ,  $c = R_{\text{vir}}/r_s = 18$ , and  $r_\odot = 8$  kpc. The Battaglia et al. NFW extremal profiles and corresponding GC  $\mathcal{J}$  are consistent with those from CU, see Eq. (7). The CU and Battaglia et al. NFW profiles are also consistent with and comparable to the high and low mass MW halo models of Klypin et al. [44]. In order to allow for comparisons with previous work, we also evaluate the constraints for the HESS GR for the case of the canonical NFW halo with  $\rho_\odot = 0.3 \text{ GeV cm}^{-3}$ ,  $R_\odot = 8.5$  kpc,  $r_s = 20$  kpc, where  $\mathcal{J}_{\Delta\Omega, \text{HGR}} = 1620$ , and the constraint in parameter space is plotted as a dotted line in Fig. 2.

Our results are less stringent for the Einasto case compared to Refs. [24, 32] because the signal used in that work did not remove the signal from the background subtraction region. Note also that our minimal case of a ‘‘CU Einasto Minimum’’ is significantly more stringent in its constraints than the adopted values in, *e.g.* Refs. [13, 14] which adopted inaccurate MW profiles from Ref. [55] which had known insufficiencies in numerical mass resolution as discussed above. We do not include here constraints from the smaller region HESS GC observations presented in Ref. [61] since they are weaker than the HESS GR observations for nearly all channels and regions in parameter space [32].

#### D. The Dark Matter Signal in the Isotropic Diffuse Background

The MW halo itself contributes to the isotropic background in an irreducible fashion due to the smooth and

unresolved portion of the MW halo. We use a very conservative limit in the required contribution of the MW Galactic halo to the isotropic diffuse background. Specifically, we assume that the entire diffuse MW signal is at minimum the value opposite the GC from a smooth halo, with a minimal substructure boost. We take that  $\mathcal{J}_{\Delta\Omega}$  is given by the anti-GC  $\mathcal{J}(0, 180^\circ)$  averaged over the full diffuse observation region  $\Delta\Omega$ ,  $\mathcal{J}_{\text{Iso}} \simeq 0.62$ . The signal towards the most Galactic-centric portion of the Fermi-LAT diffuse observation region is over two orders of magnitude larger than that away from the GC,  $\mathcal{J}(10^\circ, 0) \simeq 78$ . Therefore, our approach is extremely conservative, and leads to a robust bound since the removal of a spatial dependence in the Fermi-LAT diffuse spectrum may remove spatially-dependent components of the predicted signal.

A cold dark matter halo necessarily has enhanced annihilation from substructure in the dark matter halo. Early work had found MW substructure to contribute to boost factors of the total MW annihilation signal at over two orders of magnitude greater than the smooth halo contribution [62]. More recent work from the Aquarius simulations find similar boost factors at 232 times the smooth contribution [63]. The minimal level of enhancement from numerically resolved substructure has been found to be a factor of  $\sim 2$  from the Via Lactea and Via Lactea II simulations [64, 65]. However, substructure is expected to exist in CDM halos at potentially over twenty orders of magnitude in mass scale below a MW parent halo. Therefore, we go beyond the approximations from resolution limitations.

In order to provide a conservative estimate of the enhancement of annihilation due to unresolved substructure in the Fermi-LAT observation, we employ the analytic density probability distribution function (PDF) proposed by Kamionkowski & Koushiappas [66]. This method was recently applied to the enhancement of annihilation signals in MW-type halos with a calibration of the PDF with the Via Lactea II (VL-II) simulations [67]. That work found typical boost factors for the full MW halo are approximately 17.

In order to quantify the lower limit of the boost factor, we extremize the PDF to the lowest values consistent with the CDM halo calibration. The mean halo density from the PDF is given by

$$\begin{aligned} \bar{\rho}(r) &= \int_0^{\rho_{\text{max}}} \rho P(\rho) d\rho \\ &= f_s \rho_h + \\ &\quad (1 - f_s) \rho_h \begin{cases} \frac{1+\alpha}{\alpha} \left[ 1 - \left( \frac{\rho_{\text{max}}}{\rho_h} \right)^{-\alpha} \right]; & \alpha = 0, \\ (1 - f_s) \rho_h \ln \left( \frac{\rho_{\text{max}}}{\rho_h} \right); & \alpha \neq 0. \end{cases} \end{aligned} \quad (9)$$

The fraction  $f_s$  of the halo volume is filled with a smooth dark matter component with density  $\rho_h$ . The power law tail is calibrated to simulations to be

$$(1 - f_s) = 7 \times 10^{-3} \left( \frac{\bar{\rho}(r)}{\bar{\rho}(r = 100 \text{ kpc})} \right)^{-0.26}, \quad (10)$$

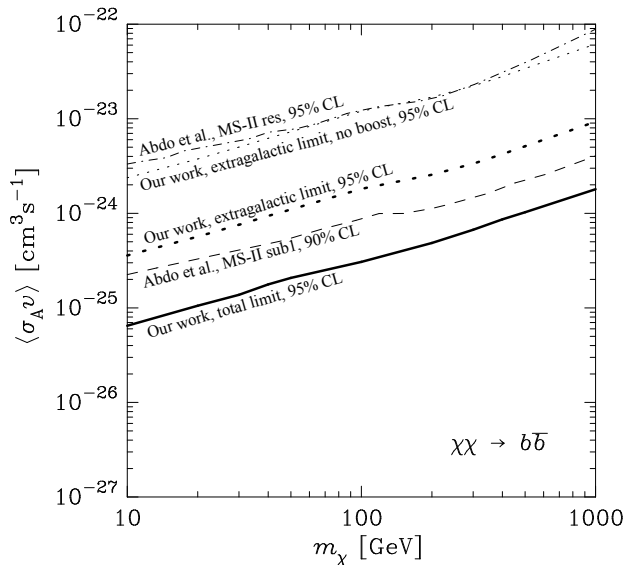


FIG. 3: Shown is a comparison of our work to the Fermi-LAT collaboration, Abdo et al. [12] constraints from the extragalactic signal in the diffuse extragalactic background from dark matter annihilation into the  $b\bar{b}$  final state. Our limits from the extragalactic background with not boost enhancement of annihilation are comparable to and consistent with that of the Abdo et al. “MS-II Res” model due to similar chosen halo mass cut-off values. Our total 95% CL limit shown here and used in Fig. 2 comes from Galactic and extragalactic contributions, with a conservative boost factor, as described in the text. Shown also is our 95% extragalactic limit alone, and the conservative model in Abdo et al. of “MS-II sub1.”

for radii greater than 20 kpc, where the overwhelmingly dominant portion of the substructure boost arises. The normalization of this tail is lower at smaller radii,  $\lesssim 20$  kpc, but the contribution to the cumulative boost from these radii is minimal. Simulations find that  $\alpha = 0 \pm 0.1$ .

The definition of the annihilation boost factor including the CDM density PDF, as a function of galactic radius is

$$B(r) = \frac{\int \rho^2 dV}{\int [\bar{\rho}(r)]^2 dV} = \int_0^{\rho_{\max}} P(\rho, r) \frac{\rho^2}{[\bar{\rho}(r)]^2} d\rho. \quad (11)$$

Explicitly, for this PDF, the boost factor is

$$B(r) = f_s e^{\Delta^2} + (1 - f_s) \frac{1 + \alpha}{1 - \alpha} \left[ \left( \frac{\rho_{\max}}{\rho_h} \right)^{1 - \alpha} - 1 \right]. \quad (12)$$

The first term  $f_s e^{\Delta^2}$  is due to the variation in the smooth component, and since  $\Delta \lesssim 0.2$  from simulations, it contributes to the overall boost factor by only a few percent and we ignore it. The second term is the boost factor due to substructure. The total boost in the galactic halo is

$$B(< R) = \frac{\int_0^R B(r) \rho(r)^2 r^2 dr}{\int_0^R \rho(r)^2 r^2 dr} \quad (13)$$

We take the extremal case to be where the slope of the power-law tail is steeper than the mean found in simulations,  $\alpha = 0.1$ . We take  $\rho_{\max}$  to be  $\rho_s$  of the earliest forming halos, which have low concentrations  $c \approx 2 - 5$ , which for centrality of this concentration distribution we take  $c = 3.5$ , forming at  $z_c = 40$ . Note that using  $\rho_s$  is extremely conservative since the smallest subhalos likely have cuspy profiles themselves that reach densities much higher than their scale density  $\rho_s$ . The integral, Eq. (13) must be evaluated numerically, and for our adopted conservative case is

$$B(< R_{\text{vir}}) = 6.6, \quad (14)$$

for  $R_{\text{vir}} = 255$  kpc. Note that this total boost is significantly lower than typically found in analytic extrapolations of MW halos which find boost factors of over two orders of magnitude. We employ this minimal boost factor, Eq. (14), in our signal calculations. It should be noted that the boost in the local (solar) region is minimal, on average, but including the boost due to substructure can affect and improve the modeling of leptonic cosmic-ray annihilation signals [67, 68].

A similar modeling to the one we adopt here of the density PDF calibrated to cosmological volume  $(100 \text{ Mpc}/h)^3$  simulations found larger scatter of the power law tail at mass scales approaching MW scale halos with boost factors between 2 and 2000 [69]. The mass resolution of the Millenium Simulation II (MS-II) employed in Ref. [69] (particle mass  $6.89 \times 10^6 M_\odot/h$ ) is approximately 2400 times less than that in VL-II (particle mass  $4100 M_\odot$ ), and the MS-II results did not extend to PDF resolution of MW size halos. This may contribute to the increased PDF scatter for lower mass halos, and therefore we adopt the VL-II calibrated PDF of Ref. [67]. Note that a complete systematic analysis of the lower limit of the substructure PDF contribution to the boost has not been performed since some of the earliest work on substructure boost factors, which found total boost scatter at the level of 40% [62]. Such a lower scatter is consistent with what we find, Eq. (14).

The cosmological contribution to the isotropic diffuse  $\gamma$ -ray background from annihilating dark matter has been studied for some time [70, 71]. The diffuse flux from annihilation in cosmological extragalactic halos is

$$\frac{d\Phi_\gamma}{dE} = \frac{\langle\sigma_A v\rangle}{2} \frac{c}{\Delta \Omega_{\text{obs}} H_0} \frac{(f_{\text{DM}} \Omega_m)^2 \rho_{\text{crit}}^2}{m_\chi^2} \times \int_0^{z_{\text{up}}} \frac{f(z)(1+z)^3}{h(z)} \frac{dN(E')}{dE'} e^{-\tau(z, E')} dz, \quad (15)$$

where  $H_0 = 70 \text{ km s}^{-1} \text{ Mpc}^{-1}$  is the Hubble constant,  $\Omega_m$  is the matter density in units of the critical density,  $\rho_{\text{crit}}$ , and the fraction of matter in dark matter is  $f_{\text{DM}} = \Omega_{\text{DM}}/(\Omega_{\text{DM}} + \Omega_b) \approx 0.833$ , where the fraction of critical density of the dark matter we take is  $\Omega_{\text{DM}} = 0.237$ , and baryon density  $\Omega_b = 0.0456$  [50]. The uncertainties in the halo modeling are much larger than the errors on the cosmological parameters we adopt



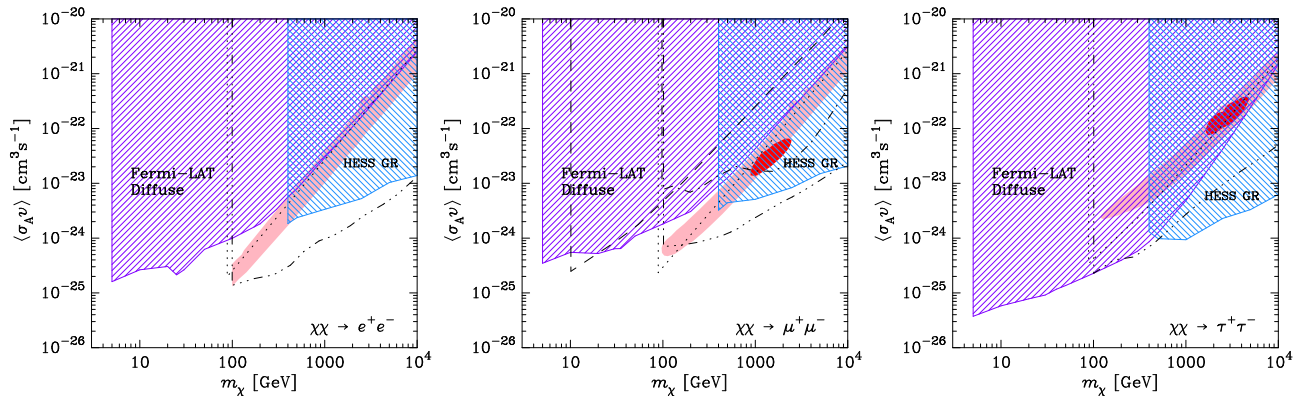


FIG. 4: Shown are constraints on regions of parameter space in annihilating dark matter models consistent with interpretations of the PAMELA positron excess (light pink region in all panels), and feature in the Fermi-LAT  $e^+/e^-$  spectrum (red region in  $\mu^+\mu^-$  and  $\tau^+\tau^-$  panels), from Ref. [24] (all 99% CL). All MW constraints and signals are for Einasto profiles, and at 95% CL. Our analysis of the Fermi-LAT isotropic diffuse background is shown along with our reanalysis of constraints from HESS observations of the Galactic Ridge (labeled HESS GR). We show several other recent constraints for comparison: ICS radiation constrained by Fermi-LAT data from the  $3^\circ \times 3^\circ$  Galactic center exclude the region within the triple-dot-dashed regions in all panels [9]; Galactic radio synchrotron observations exclude the region within the dotted line, in all panels [24]; in the central  $\mu^+\mu^-$  panel, we show the exclusion regions final state radiation constraints in Fermi-LAT observations of Draco (dashed line), and ICS radiation constraints from Fermi-LAT observations of Ursa Minor (dot-dashed line) [7]. All PAMELA models with  $m_\chi \lesssim 1$  TeV are firmly excluded by the lack of a  $\gtrsim 20\%$  drop in the Fermi  $e^+/e^-$  spectrum below 1 TeV [24].

here. However, much previous work sets  $f_{\text{DM}} = 1$ , which overestimates the extragalactic annihilation signal by approximately 30%. We take a flat universe, with  $\Omega_\Lambda$  and  $h(z) = [(1+z)^3\Omega_m + \Omega_\Lambda]^{1/2}$ . The factor  $e^{-\tau(z, E')}$  takes into account attenuation of  $\gamma$ -rays along cosmological distances, for which we use the results of Gilmore et al. [72]. The factor  $f(z)$  accounts for the increase in density squared during halo growth and the redshift evolution of the halo mass function. We adopt a fit to this evolution such that [71, 73, 74]

$$f(z) = f_0 10^{0.9[\exp(-0.9z) - 1] - 0.16z}. \quad (16)$$

The halo internal density profile sets  $f_0$ , and for the Einasto case, we find  $f_0 \simeq 3 \times 10^4$ . We also include a the boost factor here of Eq. (14) to the full extragalactic component, consistent with our adoption for the MW. The extragalactic contribution to the diffuse isotropic background is subdominant to the Galactic contribution, at the level of 10%-20% of the total signal for a given model. For comparison, shown in Fig. 3, our model of the diffuse extragalactic background is similar to that named “MS-II Res” in Ref. [12], due to a comparable low mass halo cutoff, excluding our adopted boost factor.

We redshift the energy distribution of the annihilation photons as  $E = E'/(1+z)$ , where  $E'$  is the energy of the photons at the cosmological source. Eq. (16) uses a minimal limit of the halo mass of  $10^6 M_\odot/h$ , a conservative lower limit that only uses cosmological halos known to fit cosmological determinations of the halo mass functions with no extrapolation [75]. Note that the limit from the diffuse flux greatly increases with an extrapolation to extremely low masses such as  $10^{-9} M_\odot$  employed by Hütsi et al. [34]. With our framework, we use the observed cos-

mological diffuse spectrum as the maximum amount that the annihilation signal can be at a given energy, with 95% CL limits to the full spectrum for any given  $m_\chi$ . For the 95% CL limit, we sum take the bin-summed  $\chi^2 < 1.282$  for this form of a one-sided upper limit. These limits are shown in Fig. 2.

### E. PAMELA and Fermi Electron/Positron-Spectrum Motivated Models

The PAMELA observation of an increase on the positron fraction at 10 to 100 GeV, in combination with a feature in the shape of the Fermi  $e^+/e^-$  spectrum at  $\sim 1$  TeV could be consistent with the production of the high energy  $e^+/e^-$  in the products of dark matter annihilation. Since annihilation modes to charged particles also produce photons from bremsstrahlung, the signal should also be observed or constrained by the Fermi-LAT isotropic diffuse spectrum. Channels through the quarks and massive  $W^\pm$  and  $Z$  bosons are strongly excluded by a number of observations [24]. We examine here constraints on two-body charged annihilation modes from the Fermi-LAT isotropic diffuse background, with 95% CL exclusions shown in Fig. 4. The PAMELA 99% CL preferred region is in pink, and combined Fermi- $e^+/e^-$  preferred 99% CL region in red, from Ref. [24].

We again choose the most conservative cases for the MW halo profile, as in §IID, with a shallow Einasto profile as that incorporated in Eq. (7), and high mass cutoff of the halo mass function at  $M_{\text{min}} = 10^6 M_\odot$ . The Fermi-LAT diffuse spectrum excludes a large part of the parameter space for the PAMELA and Fermi- $e^+/e^-$  99%



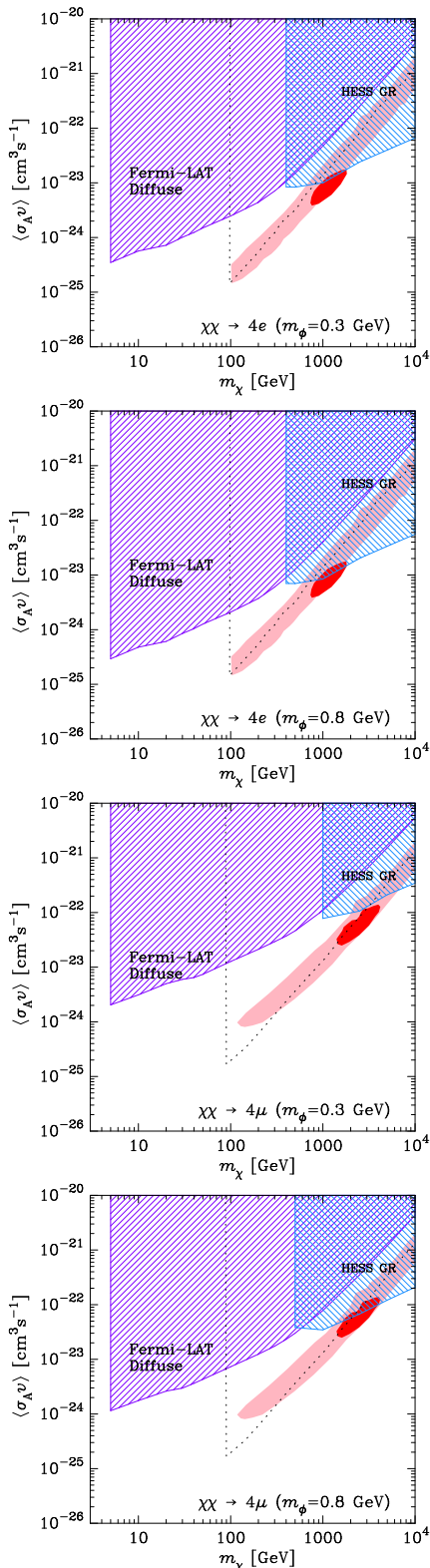


FIG. 5: Interpretations of PAMELA and Fermi  $e^+/e^-$  with an intermediate dark force carrying particle  $\phi$  allowing for dark matter annihilation into four lepton final states. The upper (lower) two panels are  $4e$  ( $4\mu$ ) final states with  $m_\phi = 0.3$  GeV and  $m_\phi = 0.8$  GeV. Galactic radio synchrotron observations exclude the region within the dotted line, in all panels [24]. All PAMELA models with  $m_\chi \lesssim 1$  TeV are firmly excluded by the lack of a  $\gtrsim 20\%$  drop in the Fermi  $e^+/e^-$  spectrum below 1 TeV [24].

CL regions, and when combined with the HESS Galactic Ridge constraints, exclude all interpretations of the PAMELA positron fraction and Fermi- $e^+/e^-$  feature as arising from dark matter annihilation into two-body standard model particle final states.

We also consider four-lepton annihilation modes that could occur through an intermediate force carrying vector or scalar boson,  $\phi$ , with mass  $m_\phi \lesssim 1$  GeV. We take scalar bosons of two cases,  $m_\phi = 0.3$  GeV and  $m_\phi = 0.8$  GeV, into either  $4e$  or  $4\mu$  final state modes. They are shown in Fig. 5. For the more massive  $\phi$  particle,  $m_\phi = 0.8$  GeV, the resultant lepton states more energetic and therefore more constrained by their final state radiation by the Fermi-LAT diffuse and HESS GR observations. For either  $\phi$  mass, there exist regions of the parameter space that are not excluded at the 95% CL level by the gamma-ray data we consider here.

For reference, we also show several other constraints that have been placed in the literature on these models also using Einasto-type profiles for the MW halo. For the two lepton modes, we show the region excluded by ICS radiation of the original final state radiation products scattering off of cosmic microwave background photons, as constrained by Fermi-LAT data from the Galactic poles (triple-dot dashed), from Ref. [9], and originally described in Ref. [76]. We also show the region excluded by synchrotron emission not observed in Galactic radio observations (dotted line) from Ref. [24], originally described in Ref. [32]; for the case of  $\chi + \chi \rightarrow \mu^+ + \mu^-$ , we show the exclusion regions from final state radiation constraints in Fermi-LAT observations of Draco (dashed line), and ICS radiation constraints from Fermi-LAT observations of Ursa Minor (dot-dashed line) [7]. In the four lepton modes, we show Galactic radio synchrotron constraints [24]. Also, it should be noted that all models with  $m_\chi \lesssim 1$  TeV are firmly excluded by the lack of a  $\gtrsim 20\%$  drop in the Fermi  $e^+/e^-$  spectrum below 1 TeV [24]. The ICS constraints from public data of Fermi-LAT observations towards the Galactic poles [9] are comparable to and, in many regions, stronger than our constraints, though such constraints do depend on ICS modeling of the signal in these regions.

### III. CONCLUSIONS

The LAT aboard the Fermi Gamma-Ray Space Telescope is opening a new window to detecting the nature of dark matter or constraining it. We have derived conservative constraints on WIMP dark matter annihilation cross-sections for all standard model channels arising from the observed isotropic diffuse background by the Fermi-LAT. We have also re-examined constraints from the HESS Galactic ridge observation. In contrast with previous work, our methods use very conservative models for the cosmological and halo structure giving rise to the signal, while still remaining consistent with structure formation in a cold dark matter framework of a WIMP

candidate. We use such conservative models in the dark matter halo profile in the Galactic signal contribution, and conservative lower-limits to the surviving halo mass function in the Galactic and extragalactic contributions to the isotropic diffuse background. For example, we do not consider isothermal halo profiles which do not arise in any CDM halo formation calculations.

Our conservative models are therefore stringent and robust constraints on any WIMP-like annihilating dark matter particle candidates. The constraints are at or near the thermal cross-section for annihilation to hadronic modes, quarks and gluons. For low masses,  $5 \text{ GeV} \lesssim m_\chi \lesssim 10 \text{ GeV}$ , the constraints exclude the expected thermal-annihilation scale  $\langle\sigma_{\text{A}v}\rangle \approx 3 \times 10^{-26} \text{ cm}^3 \text{ s}^{-1}$  into hadronic final states. Such low masses are not *a priori* excluded by previous particle physics or cosmological constraints [77, 78]. Therefore, such constraints are approaching an observational lower bound on the dark matter mass for the thermal-relic WIMP. The constraints from the isotropic diffuse background presented here are more stringent than the constraints from the diffuse background limits of the Fermi-LAT collaboration when including only the extragalactic component [12], and comparable to Fermi observations towards dwarf galaxies [7],

galaxy clusters [79], and the Galactic poles [9], while being more stringent than full-sky photon limit methods [8]. With increased integration time over the life of the Fermi Gamma-Ray Space Telescope and further constraints on dark matter structure in local and extragalactic sources, the isotropic diffuse spectrum or other Fermi-LAT observations will either reveal the  $\gamma$ -ray products of WIMP-like dark matter annihilation, or exclude this class of candidates.

## Acknowledgments

We would like to thank John Beacom, Steve Blanchet, Ilias Cholis, Marla Geha, Michael Gustafsson, Pat Harding, Ted Jacobson, Andrey Kravtsov, Julie McEnery, Stefano Profumo, Jenny Siegal-Gaskins, and Ravi Sheth for useful discussions. In particular, we thank Julie McEnery, Michael Gustafsson and the Fermi Collaboration for helping resolve an error in an earlier version of this work. KA is partially supported by NSF Grant PHY-0757966; ZC is supported by NSF Grant PHY-0801323; CK is supported by grant DOE DE-FG02-96ER50959.

- 
- [1] F. Zwicky, *Helv. Phys. Acta* **6**, 110 (1933).
  - [2] G. Jungman, M. Kamionkowski, and K. Griest, *Phys. Rept.* **267**, 195 (1996), arXiv:hep-ph/9506380.
  - [3] G. Bertone, D. Hooper, and J. Silk, *Phys. Rept.* **405**, 279 (2005), arXiv:hep-ph/0404175.
  - [4] V. Springel *et al.*, *Nature* **456**, 73 (2008), arXiv:0809.0894.
  - [5] E. A. Baltz *et al.*, *JCAP* **0807**, 013 (2008), arXiv:0806.2911.
  - [6] P. Scott *et al.*, (2009), arXiv:0909.3300.
  - [7] A. A. Abdo *et al.*, (2010), arXiv:1001.4531.
  - [8] M. Papucci and A. Strumia, (2009), arXiv:0912.0742.
  - [9] M. Cirelli, P. Panci, and P. D. Serpico, (2009), arXiv:0912.0663.
  - [10] The Fermi-LAT, A. A. Abdo *et al.*, *Phys. Rev. Lett.* **104**, 101101 (2010), arXiv:1002.3603.
  - [11] J. F. Navarro, C. S. Frenk, and S. D. M. White, *Astrophys. J.* **490**, 493 (1997), arXiv:astro-ph/9611107.
  - [12] Fermi-LAT, A. A. Abdo *et al.*, (2010), arXiv:1002.4415.
  - [13] N. F. Bell and T. D. Jacques, *Phys. Rev.* **D79**, 043507 (2009), arXiv:0811.0821.
  - [14] G. D. Mack, T. D. Jacques, J. F. Beacom, N. F. Bell, and H. Yuksel, *Phys. Rev.* **D78**, 063542 (2008), arXiv:0803.0157.
  - [15] HEAT, S. W. Barwick *et al.*, *Astrophys. J.* **482**, L191 (1997), arXiv:astro-ph/9703192.
  - [16] AMS-01, M. Aguilar *et al.*, *Phys. Lett.* **B646**, 145 (2007), arXiv:astro-ph/0703154.
  - [17] PAMELA, O. Adriani *et al.*, *Nature* **458**, 607 (2009), arXiv:0810.4995.
  - [18] E. A. Baltz, J. Edsjo, K. Freese, and P. Gondolo, *Phys. Rev.* **D65**, 063511 (2002), arXiv:astro-ph/0109318.
  - [19] I. Cholis, L. Goodenough, D. Hooper, M. Simet, and N. Weiner, *Phys. Rev.* **D80**, 123511 (2009), arXiv:0809.1683.
  - [20] J. Chang *et al.*, *Nature* **456**, 362 (2008).
  - [21] The Fermi LAT, A. A. Abdo *et al.*, *Phys. Rev. Lett.* **102**, 181101 (2009), arXiv:0905.0025.
  - [22] M. Cirelli, M. Kadastik, M. Raidal, and A. Strumia, *Nucl. Phys.* **B813**, 1 (2009), arXiv:0809.2409.
  - [23] L. Bergstrom, J. Edsjo, and G. Zaharijas, *Phys. Rev. Lett.* **103**, 031103 (2009), arXiv:0905.0333.
  - [24] P. Meade, M. Papucci, A. Strumia, and T. Volansky, (2009), arXiv:0905.0480.
  - [25] I. Cholis, L. Goodenough, and N. Weiner, *Phys. Rev.* **D79**, 123505 (2009), arXiv:0802.2922.
  - [26] N. Arkani-Hamed, D. P. Finkbeiner, T. R. Slatyer, and N. Weiner, *Phys. Rev.* **D79**, 015014 (2009), arXiv:0810.0713.
  - [27] M. Baumgart, C. Cheung, J. T. Ruderman, L.-T. Wang, and I. Yavin, *JHEP* **04**, 014 (2009), arXiv:0901.0283.
  - [28] A. Katz and R. Sundrum, *JHEP* **06**, 003 (2009), arXiv:0902.3271.
  - [29] J. Zavala, M. Vogelsberger, and S. D. M. White, (2009), arXiv:0910.5221.
  - [30] J. L. Feng, M. Kaplinghat, and H.-B. Yu, (2009), arXiv:0911.0422.
  - [31] M. R. Buckley and P. J. Fox, (2009), arXiv:0911.3898.
  - [32] G. Bertone, M. Cirelli, A. Strumia, and M. Taoso, *JCAP* **0903**, 009 (2009), arXiv:0811.3744.
  - [33] R. Essig, N. Sehgal, and L. E. Strigari, *Phys. Rev.* **D80**, 023506 (2009), arXiv:0902.4750.
  - [34] G. Huetsi, A. Hektor, and M. Raidal, (2009), arXiv:0906.4550.
  - [35] A. Boulares, *Astrophys. J.* **342**, 807 (1989).
  - [36] D. Hooper, P. Blasi, and P. D. Serpico, *JCAP* **0901**, 025

- (2009), arXiv:0810.1527.
- [37] H. Yuksel, M. D. Kistler, and T. Stanev, Phys. Rev. Lett. **103**, 051101 (2009), arXiv:0810.2784.
- [38] S. Profumo, (2008), arXiv:0812.4457.
- [39] T. Sjostrand, S. Mrenna, and P. Z. Skands, JHEP **05**, 026 (2006), arXiv:hep-ph/0603175.
- [40] J. Mardon, Y. Nomura, D. Stolarski, and J. Thaler, JCAP **0905**, 016 (2009), arXiv:0901.2926.
- [41] J. Diemand, B. Moore, and J. Stadel, Mon. Not. Roy. Astron. Soc. **353**, 624 (2004), arXiv:astro-ph/0402267.
- [42] J. Stadel *et al.*, Mon. Not. Roy. Astron. Soc. **398**, L21 (2009), arXiv:0808.2981.
- [43] J. F. Navarro *et al.*, (2008), arXiv:0810.1522.
- [44] A. Klypin, H. Zhao, and R. S. Somerville, Astrophys. J. **573**, 597 (2002), arXiv:astro-ph/0110390.
- [45] G. Battaglia *et al.*, Mon. Not. Roy. Astron. Soc. **364**, 433 (2005), astro-ph/0506102.
- [46] R. Catena and P. Ullio, (2009), arXiv:0907.0018.
- [47] B. Moore, F. Governato, T. R. Quinn, J. Stadel, and G. Lake, Astrophys. J. **499**, L5 (1998), arXiv:astro-ph/9709051.
- [48] A. V. Maccio' *et al.*, Mon. Not. Roy. Astron. Soc. **378**, 55 (2007), arXiv:astro-ph/0608157.
- [49] K. Heitmann, P. M. Ricker, M. S. Warren, and S. Habib, Astrophys. J. Suppl. **160**, 28 (2005), arXiv:astro-ph/0411795.
- [50] E. Komatsu *et al.*, (2010), arXiv:1001.4538.
- [51] SDSS, D. J. Eisenstein *et al.*, Astrophys. J. **633**, 560 (2005), arXiv:astro-ph/0501171.
- [52] U. Seljak, A. Makarov, P. McDonald, and H. Trac, Phys. Rev. Lett. **97**, 191303 (2006), arXiv:astro-ph/0602430.
- [53] K. Abazajian and S. M. Koushiappas, Phys. Rev. **D74**, 023527 (2006), arXiv:astro-ph/0605271.
- [54] M. Viel *et al.*, Phys. Rev. Lett. **100**, 041304 (2008), arXiv:0709.0131.
- [55] A. V. Kravtsov, A. A. Klypin, J. S. Bullock, and J. R. Primack, Astrophys. J. **502**, 48 (1998), arXiv:astro-ph/9708176.
- [56] A. Klypin, A. V. Kravtsov, J. Bullock, and J. Primack, Astrophys. J. **554**, 903 (2001), arXiv:astro-ph/0006343.
- [57] HESS, F. Aharonian *et al.*, Nature **439**, 695 (2006), arXiv:astro-ph/0603021.
- [58] HESS, . F. Aharonian, Astropart. Phys. **29**, 55 (2008), arXiv:0711.2369.
- [59] M. Regis and P. Ullio, Phys. Rev. **D78**, 043505 (2008), arXiv:0802.0234.
- [60] X.-J. Bi, X.-G. He, E. Ma, and J. Zhang, (2009), arXiv:0910.0771.
- [61] HESS, M. Vivier, Hess galactic center observations, in *Talk presented at 44th Rencontres de Moriond, February 6, 2009*, 2009.
- [62] C. Calcaneo-Roldan and B. Moore, Phys. Rev. **D62**, 123005 (2000), arXiv:astro-ph/0010056.
- [63] V. Springel *et al.*, Nature **456N7218**, 73 (2008), arXiv:0809.0894.
- [64] J. Diemand, M. Kuhlen, and P. Madau, Astrophys. J. **657**, 262 (2007), arXiv:astro-ph/0611370.
- [65] M. Kuhlen, J. Diemand, and P. Madau, (2008), arXiv:0805.4416.
- [66] M. Kamionkowski and S. M. Koushiappas, Phys. Rev. **D77**, 103509 (2008), arXiv:0801.3269.
- [67] M. Kamionkowski, S. M. Koushiappas, and M. Kuhlen, Phys. Rev. **D81**, 043532 (2010), arXiv:1001.3144.
- [68] J. M. Cline, A. C. Vincent, and W. Xue, (2010), arXiv:1001.5399.
- [69] J. Zavala, V. Springel, and M. Boylan-Kolchin, Mon. Not. Roy. Astron. Soc., 453 (2010), arXiv:0908.2428.
- [70] L. Bergstrom, J. Edsjo, and P. Ullio, Phys. Rev. Lett. **87**, 251301 (2001), arXiv:astro-ph/0105048.
- [71] P. Ullio, L. Bergstrom, J. Edsjo, and C. G. Lacey, Phys. Rev. **D66**, 123502 (2002), arXiv:astro-ph/0207125.
- [72] R. C. Gilmore, P. Madau, J. R. Primack, R. S. Somerville, and F. Haardt, (2009), arXiv:0905.1144.
- [73] S. Ando, Phys. Rev. Lett. **94**, 171303 (2005), arXiv:astro-ph/0503006.
- [74] H. Yuksel, S. Horiuchi, J. F. Beacom, and S. Ando, Phys. Rev. **D76**, 123506 (2007), arXiv:0707.0196.
- [75] J. L. Tinker *et al.*, Astrophys. J. (in press) (2008), arXiv:0803.2706.
- [76] M. Cirelli and P. Panci, Nucl. Phys. **B821**, 399 (2009), arXiv:0904.3830.
- [77] D. Choudhury, H. K. Dreiner, P. Richardson, and S. Sarkar, Phys. Rev. **D61**, 095009 (2000), arXiv:hep-ph/9911365.
- [78] S. Profumo, Phys. Rev. **D78**, 023507 (2008), arXiv:0806.2150.
- [79] Fermi-LAT, A. A. Abdo *et al.*, (2010), arXiv:1002.2239.